ORIGINAL RESEARCH ARTICLE

Effect of Heat Treatment on the Microstructure and Mechanical Properties of Investment Casting Ti-1300 Alloy

YULUO LI, QIANG LIAO, YANG SONG, and YIMING YANG

The application of titanium alloys in military equipment put forward the requirement for higher strength–plasticity matching. Investment casting is a promising method for the efficient and economical processing of titanium alloys. However, research on the investment casting of higher strength–plasticity matching titanium alloys is still limited. This study systematically investigated the microstructure and mechanical properties of investment casting ultrahigh-strength Ti-1300 alloy under different heat treatment methods and process parameters. The results show that the as-cast microstructure of the investment casting Ti-1300 alloy is a coarse Widmanstätten structure, which exhibits a high ultimate tensile strength (UTS) of 1143.0 MPa with elongation (EI) close to 0. After β-solution and single-aging treatments, the UTS decreased and the EI rapidly increased. This is primarily because the width of the α_P phase was significantly increased and the orientation was more random. In addition, the UTS and yield strength (YS) increased with decreasing aging temperature, while the EI remained unchanged. This was attributed to an increase in the α_P phase content. After 880 °C β-solution and 600 °C aging, the investment casting Ti-1300 alloy exhibited optimal strength–plasticity matching, with a UTS of 949 MPa and an EI of 13.5 pct. Based on these results, to further increase the UTS of the investment casting Ti-1300 alloy, β-solution and double-aging treatment processes were designed to investigate the effect of the morphology of the α_s phase on the mechanical properties. The results show that the UTS and YS increase and the EI decreases with decreasing secondary aging temperatures. This was primarily ascribed to the width of the α_s phase decreasing with decreasing secondary aging temperatures. After 880 °C β-solution and 750 °C aging followed by 620 °C aging, the investment casting Ti-1300 alloy achieved high strength–plasticity matching, with a UTS of 1094 MPa and an EI of 7.0 pct.

https://doi.org/10.1007/s11661-024-07544-z

I. INTRODUCTION

TITANIUM and its alloys have been widely applied to aerospace, orthopedic implant and the chemical industry due to their excellent properties such as low density, high specific strength, excellent biocompatibility and good corrosion resistance.[1–4] Among them, near-β titanium alloys has received widespread attention in recent years due to their high specific strength and ultimate tensile strength (UTS) after post heat-treatment.[4,5] Presently, the most widely studied near-β titanium alloy is Ti–5Al–5Mo–5V–3Cr (Ti-5553), which has also been successfully used in the Boeing Dreamliner 787 to fabricate truck beams in landing gear modules.[6,7] Most of the literature on near-β titanium alloys is mainly focused on additive manufacturing and thermal mechanical processing, resulting in all Ti-5553 alloy components being prepared by additive manufacturing and machining or thermal mechanical processing and machining methods.[8–11]

Recently, with the rapid development of military equipment, lightweight weapons and equipment is becoming an important issue, as they affect the improvement of an individual's combat capabilities. Unlike the demand for the high-temperature mechanical properties of titanium alloys in the aerospace field, military equipment primarily requires the room-temperature mechanical properties of titanium alloys. Therefore, high-strength near-β titanium alloys are receiving widespread attention from the army. However, the high cost of both of these preparation processes limits their application in the army.[7,12,13] Thus, reducing the production cost of high-strength near-β titanium alloys is key to broadening their application field. Investment casting is a near-net-shape manufacturing method, improving material usage and reduce production

YULUO LI, QIANG LIAO, YANG SONG, and YIMING YANG are with the Western Metal Materials Co., Ltd., Xi'an 710201, Shaanxi, P.R. China. Contact e-mail: myliyuluo@163.com
Manuscript submitted May 6, 2024; accepted July 21, 2024.
Article published online August 8, 2024

costs.[13,14,15] In addition, the products produced using this method are widely used in the aviation, aerospace, and petrochemical fields, indicating that the products produced using this method have high quality and reliability.[16] Nevertheless, the cast coarse Widmanstätten structure significantly reduces the mechanical properties of investment casting near-β titanium alloys, thus making them unable to meet practical usage requirements. Therefore, regulating the microstructures and mechanical properties of investment casting near-β titanium alloys is a key scientific problem to their application. Several reports have described forged near-β titanium alloy microstructures and properties that are sensitive to hot working and post heat-treatment technologies.[17,18] However, no information is available on the regulation of the microstructure and mechanical properties of investment casting near-β titanium alloys. For near β titanium alloy products formed by hot processing, Ding *et al.* believe that near β titanium alloy should first experience the hot rolling or forging treatment to obtain discontinuous grain boundary α phase.[19] However, near-β titanium alloy products produced by investment casting cannot undergo grain hot deformation processing. Therefore, understanding the effect of post heat-treatment methods and process parameters on the microstructural evolution and mechanical properties of investment casting near-β titanium is essential for its application. Herein, we chose the novel near-β Ti–5Al–4Cr–4Mo–4V–3Zr (Ti-1300) titanium alloy developed by the Northwest Institute for Nonferrous Metal Research in China as the research object.[20–22] To understand the influence of post heat-treatment methods and process parameters on the microstructural evolution and machinal properties of investment casting Ti-1300 alloy, we designed two heat-treatment methods, β solution and single aging and β solution and double aging, and seven heat-treatment-process parameters. The results of this study contribute to understanding the effect of the morphology and volume fraction of the primary α (α_P) and secondary α (α_S) phases on the mechanical properties and to achieving strength–plasticity matching of investment casting Ti-1300 alloy.

II. EXPERIMENTAL PROCEDURE

Samples of the investment casting Ti-1300 alloy were prepared by a vacuum shell furnace. The pouring temperature and cooling time are 1800 °C and 2 hours, respectively. The dimensions of the samples were $\Phi 30 \times 150$ mm. The chemical composition of this as-cast Ti-1300 alloy was then determined using inductively coupled plasma analysis, as shown in Table I. To eliminate defects in as-cast samples, all samples were treated with hot isostatic pressing at 920 °C and 130 MPa for 2.5 h min. The β-transit temperature was metallographically measured to be approximately 830 °C. To investigate the influence of the morphology and volume fraction of the α_P and α_S phases on the machinal properties of investment casting Ti-1300 alloy, two post heat-treatment methods, β solution and single aging (named as SA) and β solution and double aging (named as SDA), and seven post-heat treatment process parameters were designed. The details of the two-post heat-treatment methods and the seven post-heat treatment process parameters are shown in Figure 1. The post heat-treatment process parameters were as follows: SA-750 (880 °C/1.5 hours + 750 °C/2 hours), SA-700 (880 °C/1.5 hours + 700 °C/2 hours), SA-650 (880 °C/1.5 hours + 650 °C/2 hours), SA-600 (880 °C/1.5 hours + 600 °C/2 hours), SDA-650 (880 °C/1.5 hours + 750 °C/2 hours + 650 °C/3 hours), SDA-620 (880 °C/1.5 hours + 750 °C/2 hours + 620 °C/3 hours), and SDA-570 (880 °C/1.5 hours + 750 °C/2 hours + 570 °C/3 hours).

Specimens for optical microscopy (OM; Axio Vert.A1; ZEISS) and scanning electron microscopy (SEM; JSM 7200F; JEOL) observations were metallographically ground, polished, and etched using Kroll's reagent (5 vol pct HF + 15 vol pct HNO_3 + 80 vol pct H_2O) for 30 s. The microstructural evolution and fracture morphologies of the different post heat-treatment methods and process parameters in the samples were then analyzed. Quantitative analysis of the microstructure characteristics was performed using Imaging Pro software. Tensile specimens were processed according to GB/T 228.1–2021 of China. Tensile tests were conducted using an Instron-type testing machine at a cross speed of 8.3×10^{-6} m/s before the yield point and a cross speed of 8.3×10^{-5} m/s after the yield point.

III. RESULTS AND DISCUSSION

A. *As-Cast Ti-1300 Alloy Microstructure and Mechanical Properties*

Figure 2 shows the microstructures, stress–strain curves, and fracture morphologies of the as-cast Ti-1300 alloy. Figure 2(a) shows that the as-cast microstructure of the Ti-1300 alloy comprises coarse β grains and a continuous α grain boundary (α_{GB}) distributed on the β-grain boundaries, marked with yellow arrows in Figure 2(a). Figures 2(a) and (b) shows that the coarse β grains comprise variously sized and oriented α colonies (α_C) composed of parallel distributions of the lamellar α_P phase and β residual (β_R) matrix, marked with yellow arrows in Figures 2(a) and (b). In addition, the α_S phase is observed in the bulk β_R matrix. To further analyze, the widths of the α_P phase were quantitatively measured using Imaging Pro software, as shown in Figure 2(c). The width distribution of the α_P phase with an 81.5 pct volume fraction ranged from 0.3 to 0.9 μm. This indicates that the microstructure of the as-cast Ti-1300 alloy is a typical coarse Widmanstätten structure, primarily owing to the low cooling rate of the investment casting process providing sufficient growth time for the α_P phase. Figure 2(d) shows the stress–strain curve of the as-cast Ti-1300 alloy. The samples broke before reaching the specified yield strength of 2 pct. The ultimate tensile strength (UTS) is 1143.0 MPa, the elongation (EI) is 1.2 pct, and the calculated average elastic modulus (E) is 105.9 GPa. According to Wen

et al.[23] report, the plasticity and strength of the TC21 alloy with a lamellar microstructure decreased as the thickness of the α_P phase sheet decreased because thin α plates decrease the size of the plastic deformation zone of the crack tip. As shown in Figures 2(a) through (c), the low EI of the as-cast Ti-1300 alloy was owing to the precipitation of the thin-layer α_P phase. To further investigate the fracture behavior, the macroscopic and microscopic fracture morphologies of the tensile sample were analyzed using SEM, as shown in Figures 2(d) through (f). The obvious tear ridges are observed in in Figure 2(d), indicating that intergranular crack propagation along the continuous α boundary distributed on β grain boundaries are the dominant failure mechanism in the as-cast Ti-1300 alloy. To further understand the fracture mechanism, the uneven and flat areas marked with red circles in Figure 2(d) were analyzed, as shown in Figures 2(e) and (f). Secondary cracks, microvoids and dimples are observed. However, the dimples are small and shallow, meaning that the tear area has low toughness. As shown in Figure 2(f), the intergranular fracture area displays shell-shaped dimples, indicating that the brittleness of the as-cast Ti-1300 alloy results in its inability to be applied in engineering practice. Therefore, the regulation of the microstructure and mechanical properties using post-heat treatment is a key issue for determining whether investment Ti-1300 alloy can be applied in engineering.

B. *Effect of SA Post heat-Treatment on the α_P Phase and Mechanical Properties*

According to published reports,[24–26] the β grains, α_C, and α_P and α_S phases in titanium alloys with multilevel microstructures significantly influence their mechanical properties. For example, Terlinde *et al.*[26] believes that a decrease in the volume fraction of the α_P phase leads to a significant decrease in plasticity in Ti–10V–2Fe–3Al titanium alloy owing to a soft α_P phase and hard β phase. Because β grain size cannot be effectively regulated using post heat-treatment methods, we investigated the influence of post heat-treatment process parameters on the α_C and α_P phase and analyzed the effect of the α_C and α_P phase on the mechanical properties of investment casting Ti-1300 alloy. The detailed process parameters for samples SA-750, SA-700, SA-650, and SA-600 are shown in Figure 1(a).

Table I. Chemical Composition of the Investment Casting Ti-1300 Alloy

Element	Ti	Al	Mo	Cr	V	Zr	O
Wt Pct	bal.	5.0	3.91	3.87	3.81	2.97	0.1

Figure 3 shows the SEM images and widths of the α_P plates of the investment casting Ti-1300 alloy after SA post heat-treatment method, and the detail parameters is shown in Figure 1(a). Figures 3(a), (d), (g), and (j) shows that the grain-boundary α phase transition thins and becomes discontinuous with decreasing annealing temperature, and no obvious α_C was observed except in some grains of SA-700 sample. Only the α_P phase precipitates in β grains after SA post heat-treatment, as shown in Figures 3(b), (e), (h), and (k). To further analyze the volume fractions and widths of the α_P plates shown in Figures 3(b), (e), (h), and (k), they were measured using Imaging Pro software, as shown in Figures 3(c), (f), (i), and (l). The volume fractions of the α_P phase in the samples were 36.9, 61.7, 63.9, and 66.3 pct, indicating that decreasing the aging temperature is beneficial for the precipitation of the α_P phase. The β phase is a high-temperature metastable phase and the α phase is a room-temperature stable phase in titanium alloys. In addition, after the completion of the β-solution treatment at 880 °C for 1.5 hours, the furnace was cooled to the aging temperature at a cooling rate of approximately 1 °C/min, which means that a low aging temperature results in a long holding time. Thus, the volume fractions of the α_P phases increased with decreasing aging temperature.

The main widths of α_P plates in these samples were between 1.0 and 2.5 μm, between 0.5 and 2.5 μm, between 0.9 and 1.8 μm, and between 0.8 and 2.0 μm. Compared with the as-cast state, not only the width of

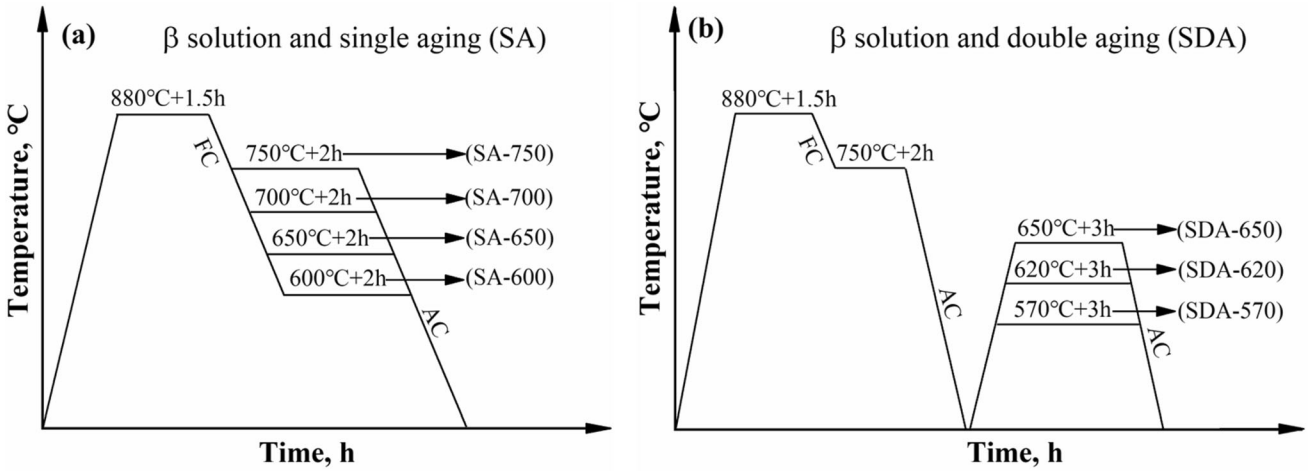

Fig. 1—Investment casting Ti-1300 alloy post heat-treatment process parameters: (*a*) SA and (*b*) SDA. FC, furnace cooling; AC, air cooling.

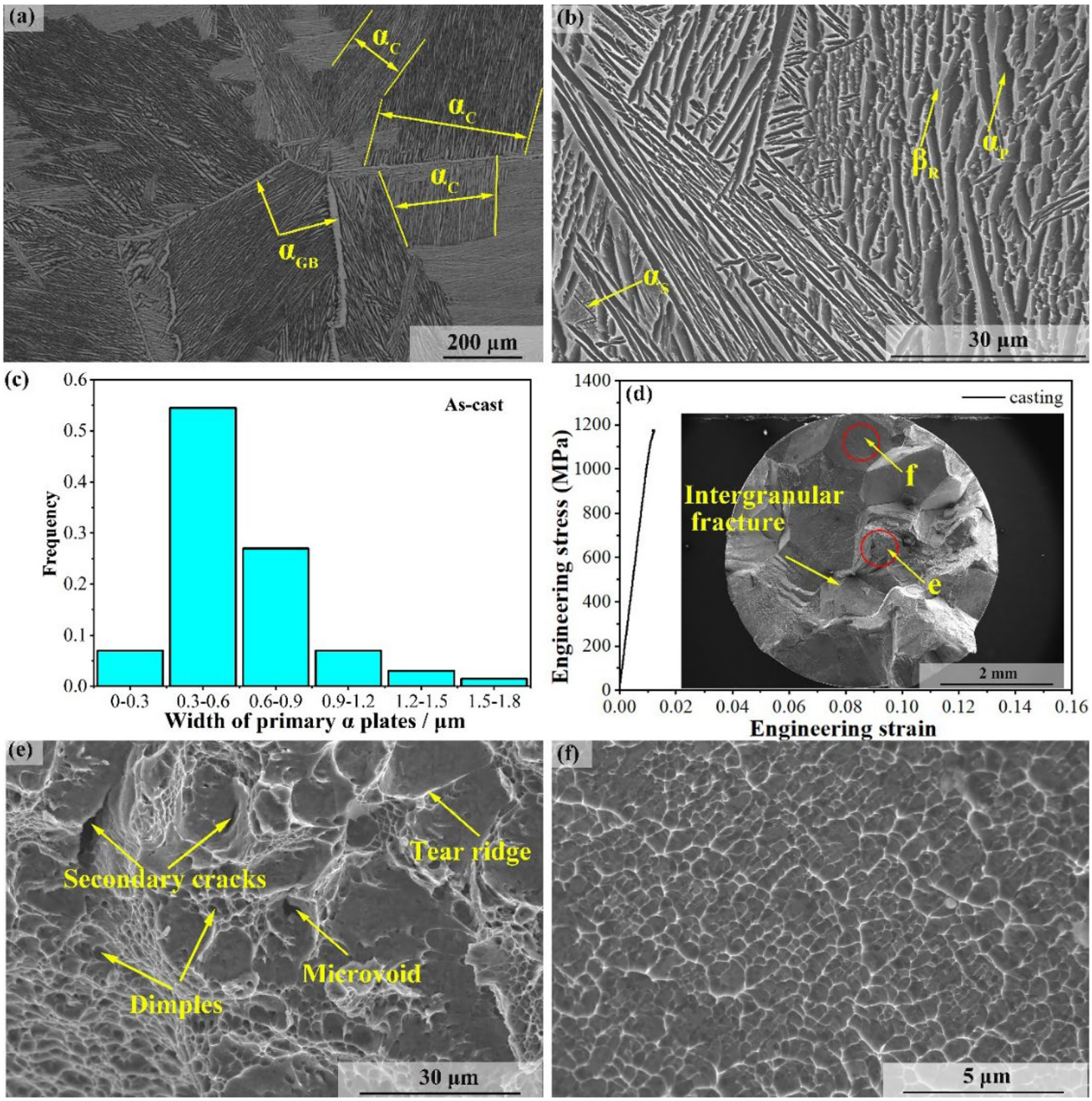

Fig. 2—Microstructures, stress–strain curve and fracture morphologies of the investment casting Ti-1300 alloy. (*a*) OM and (*b*) SEM microstructures. (*c*) Width of the primary α plates. (*d*) Stress–strain curve. Inserted image in (d), (*e*) and (*f*) fracture morphologies. α_{GB}, continuous α grain boundary distributed on the β-grain boundaries. α_C, α colonies composed of parallel distributions of the lamellar primary α (α_P) phase and β residual (βR) matrix. α_S, secondary α.

the α_P plates after SA post heat-treatment increases, but also the distribution range becomes larger. Although the widths of the α_P plates in these samples after SA post heat-treatment did not significantly change, the distribution interval frequency of the α_P phases significantly change. According to Wang *et al.*,[27] as the temperature difference between the aging temperature and solution temperature increases, the driving force of the $\beta \rightarrow$ a phase transformation increases during treatment, which is conducive to the formation of nuclei in random directions. However, a high nucleation rate limits the α_P-phase growth of partial preferential nucleation. Therefore, the distribution interval frequency of the α_P phase decreased with decreasing primary aging temperature, except for SA-700. In general, after the SA post heat-treatment, the morphology of the α_P phase in the investment casting Ti-1300 alloy can be effectively regulated.

Figure 4 shows the variation in the tensile properties of the investment casting Ti-1300 alloy with annealing temperature. As shown in Figure 4(a), the engineering stress of the SA-750 sample decreases after the yield

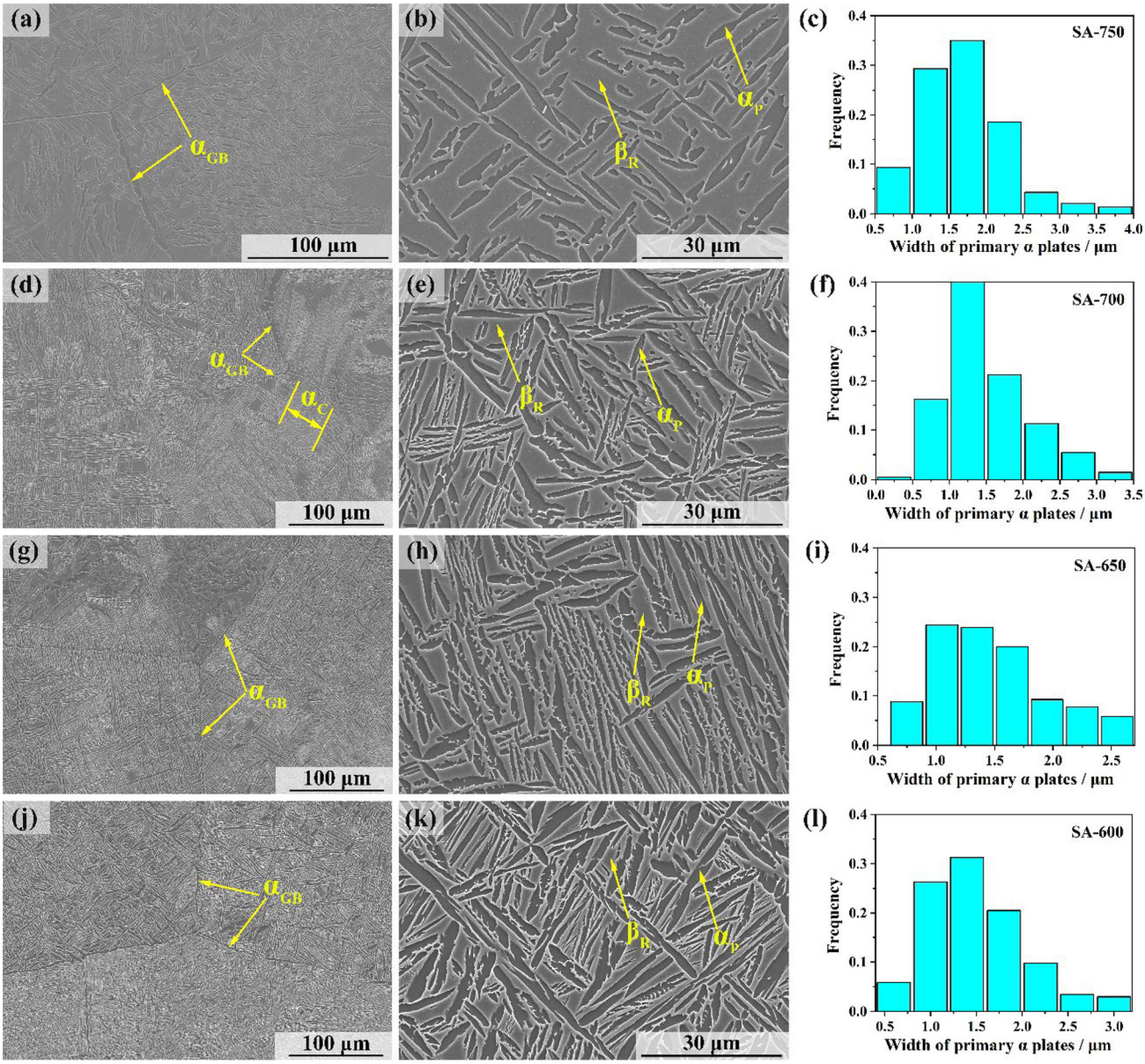

Fig. 3—SEM images of the investment casting Ti-1300 alloy after SA post heat-treatment. (*a*) to (*c*) SA-750, (*d*) to (*f*) SA-700, (*g*) to (*i*) SA-650, and (*j*) to (*l*) SA-600. α_{GB}, continuous α grain boundary distributed on the β-grain boundaries. α_C, α colonies composed of parallel distributions of the lamellar primary α (α_P) phase and β residual (βR) matrix. α_S, secondary α.

point as the engineering strain increases. Figure 3(b) shows that the microstructure of SA-750 sample is composed of 63.1 pct bcc-structure β phase and 36.9 pct hcp-structure α phase. According to Schwab,[28] this stress drop is common for materials with a bcc crystal structure at low deformation temperature. This effect can be explained by two theories. First, the static theory, describes discontinuous yielding as the dissociation of dislocations from a solute atomic environment.[29] Second, the dynamic theory, assumes that grain boundaries act as a source of new mobile dislocations.[30] Both theories are based on the low dislocation density of materials.[31] Herein, all Ti-1300 alloy samples were obtained by investment casting without any thermal mechanical processing. Thus, we speculated that all samples have a low dislocation density, which meets the basic requirements of these two theories. The engineering stresses of the other three samples remained unchanged after the yield point. According to published reports,[22,32] α/β interfaces can hinder the dislocation slip between these two phases and further act as stress concentrators. Based on the statistical results shown in Figures 3(f), (i), and (l), the hcp-structure primary α phase content in these three samples is greater than 60 pct, meaning that these three samples have a high density of α/β interfaces. A high-volume fraction of the α_P phase is beneficial for preventing stress decreasing with strain in near-β titanium alloys.

Figure 4(b) shows that the UTS and yield strength (YS) slightly increase with decreasing aging temperature

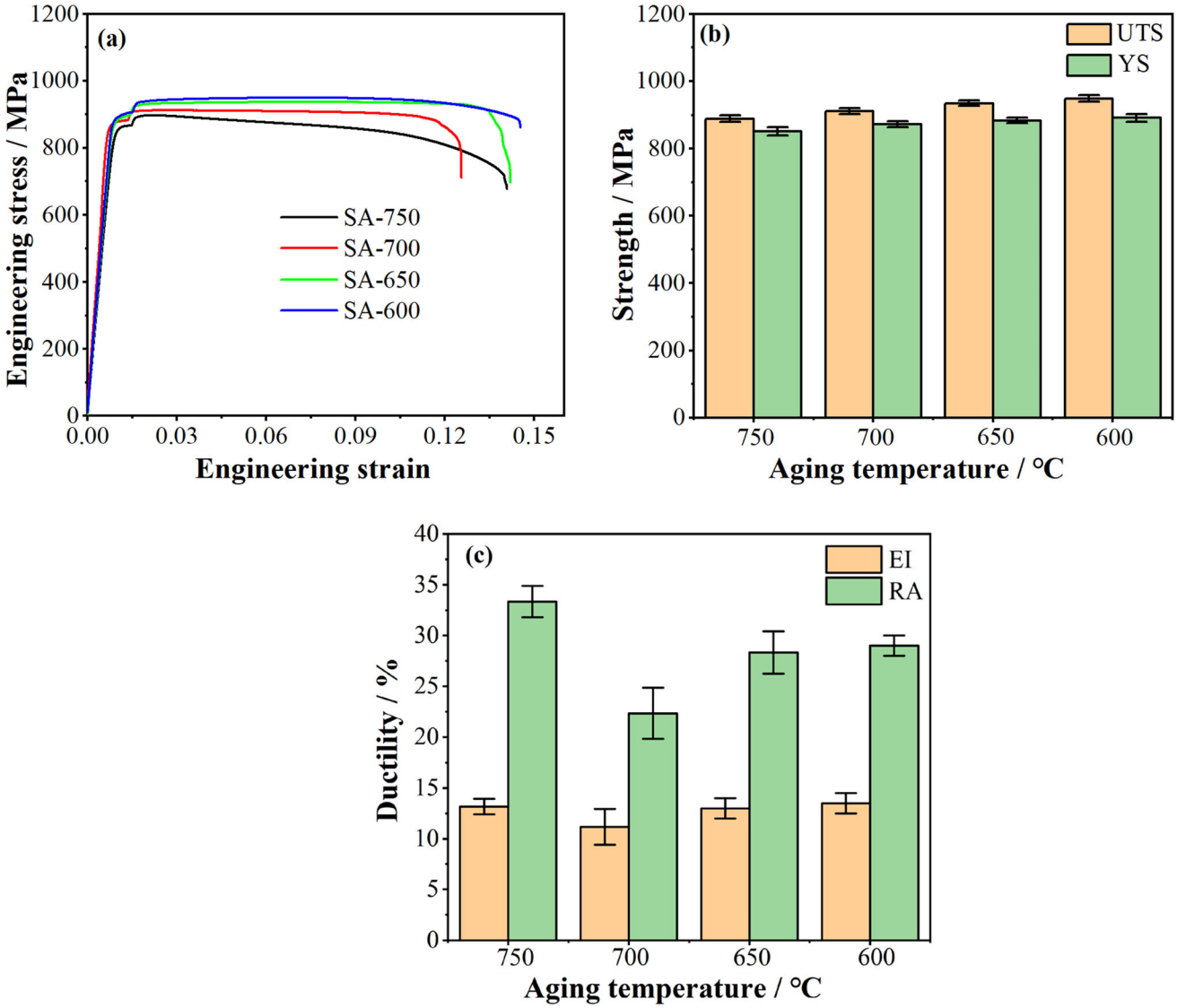

Fig. 4—Tensile properties of the Ti-1300 alloy at different annealing temperatures. (*a*) Stress–strain curves, (*b*) Ultimate Tensile strength (UTS) and yield strength (YS), and (*c*) Elongation (EI) and reduction area (RA).

from 750 °C to 600 °C. The UTS and YS of the alloy increased by approximately 6.7 and 4.7 pct, respectively. Based on the results shown in Figure 3, the increase in UTS and YS can be ascribed to the increasing volume fraction of the α_P phase. This means that the α_P phase is harder than the β phase. However, Terlinde *et al.*[26] show that the α_P phase is softer than the β phase in Ti–10 V–2Fe–3Al titanium alloy. This indicates that the degree of softness or hardness between the α_P and β phases vary in different alloys. Figure 4(c) shows that the EI and reduction area (RA) remained unchanged, except for SA-700. The decreasing EI and RA of SA-700 was owing to the formation of coarse Widmanstätten structures in some β grains, as shown in Figure 3(d). Briefly, compared with the as-cast Ti-1300 alloy mechanical properties, after SA post heat-treatment, the strength of the investment casting Ti-1300 alloy decreased, whereas the plasticity significantly increased. Wang *et al.*[27] show that a small α_P phase width increases dislocation motion resistance. In addition, by comparing Figures 2(b) and 3(b), (e), (h), and (h), the orientation relationship of the α_P phase is no longer apparent, which is conducive to hindering crack diffusion.

To further investigate the influence of microstructure after SA post heat-treatment on fracture behavior, the tensile fracture morphologies of the four samples were investigated using SEM, as shown in Figure 5. Figures 5(a), (c), (e), and (g) show that the macroscopic fracture morphologies of these samples are uneven and have obvious tearing marks. Moreover, very few intergranular fractures were observed in SA-600, indicating that the fracture mechanism of these four samples is transgranular fracture. For further study, the typical regions shown in Figures 5(a), (c), (e), and (g) (marked with red circles) were analyzed, as shown in Figures 5(b), (d), (f), and (h), respectively. The fracture morphology of these samples exhibits fractured features,

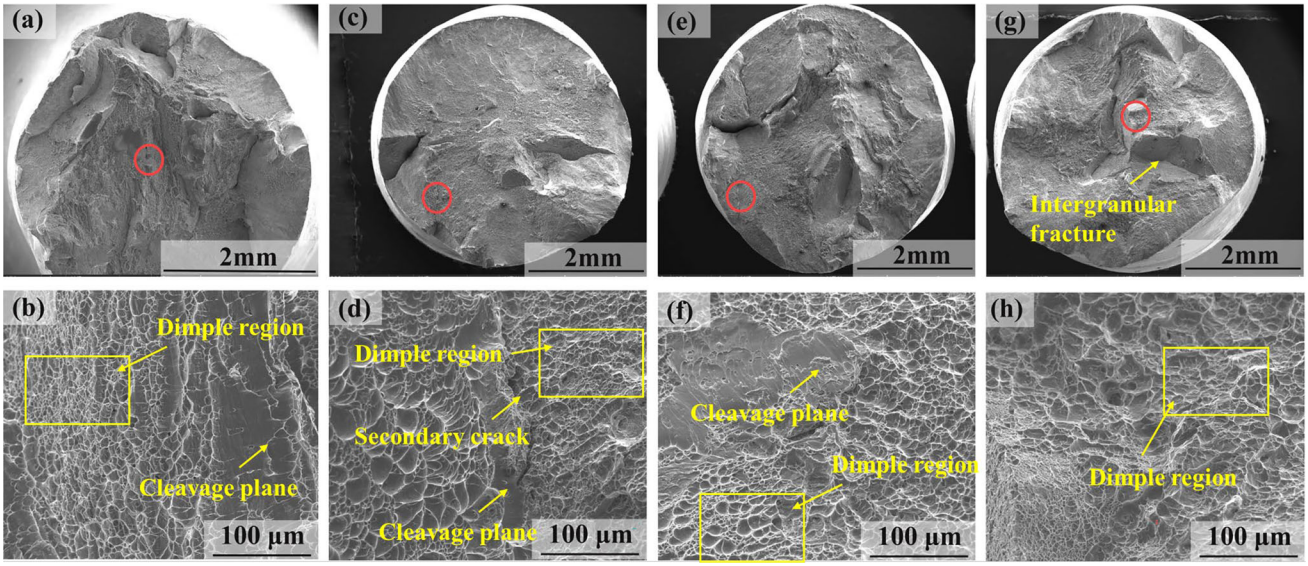

Fig. 5—Fracture morphologies of the investment casting Ti-1300 alloy after SA post heat-treatment. (*a*) and (*b*) SA-750, (*c*) and (*d*) SA-700, (*e*) and (*f*) SA-650, and (*g*) and (*h*) SA-600.

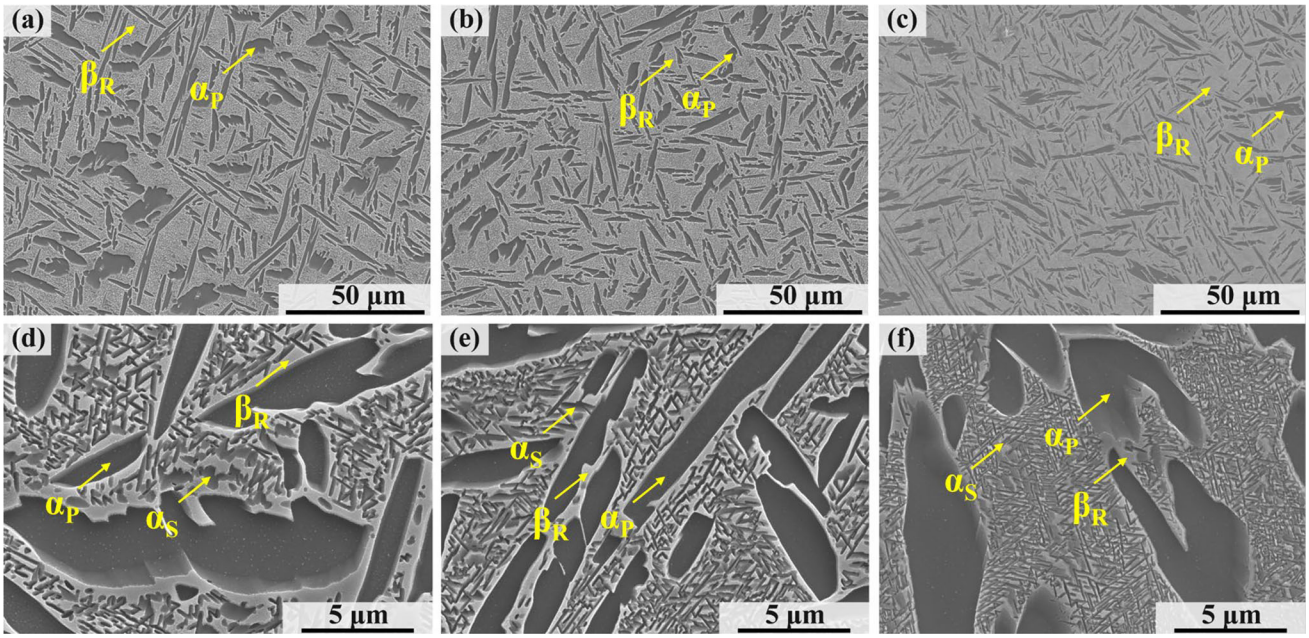

Fig. 6—SEM images of the investment casting Ti-1300 alloy after SDA post heat-treatment. (*a*) and (*d*) SDA-650, (*b*) and (*e*) SDA-620, and (*c*) and (*f*) SDA-570. α_P, primary α. β_R, β residual. α_S, secondary α.

including dimples, cleavage planes, and secondary cracks. However, it is mainly dominated by dimples, which are large and deep. Large and deep dimples can extend crack propagation paths and propagation time.[26–28] Therefore, these samples exhibit high EI and RA. By contrast, the mechanical properties of the investment casting Ti-1300 alloy can be effectively improved by adjusting the morphology and volume fraction of the α_P phase.

C. *Effect of SDA Post heat-Treatment on the α_S Phase and Mechanical Properties*

Based on the above analysis, it was concluded that SA-750 sample has a low volume fraction, optimal morphology of the α_P phase, and a good matching relationship between strength and plasticity. It also left enough room to study the relationship between the α_S phase and the machinal properties. We designed the SDA post heat-treatment method to investigate the

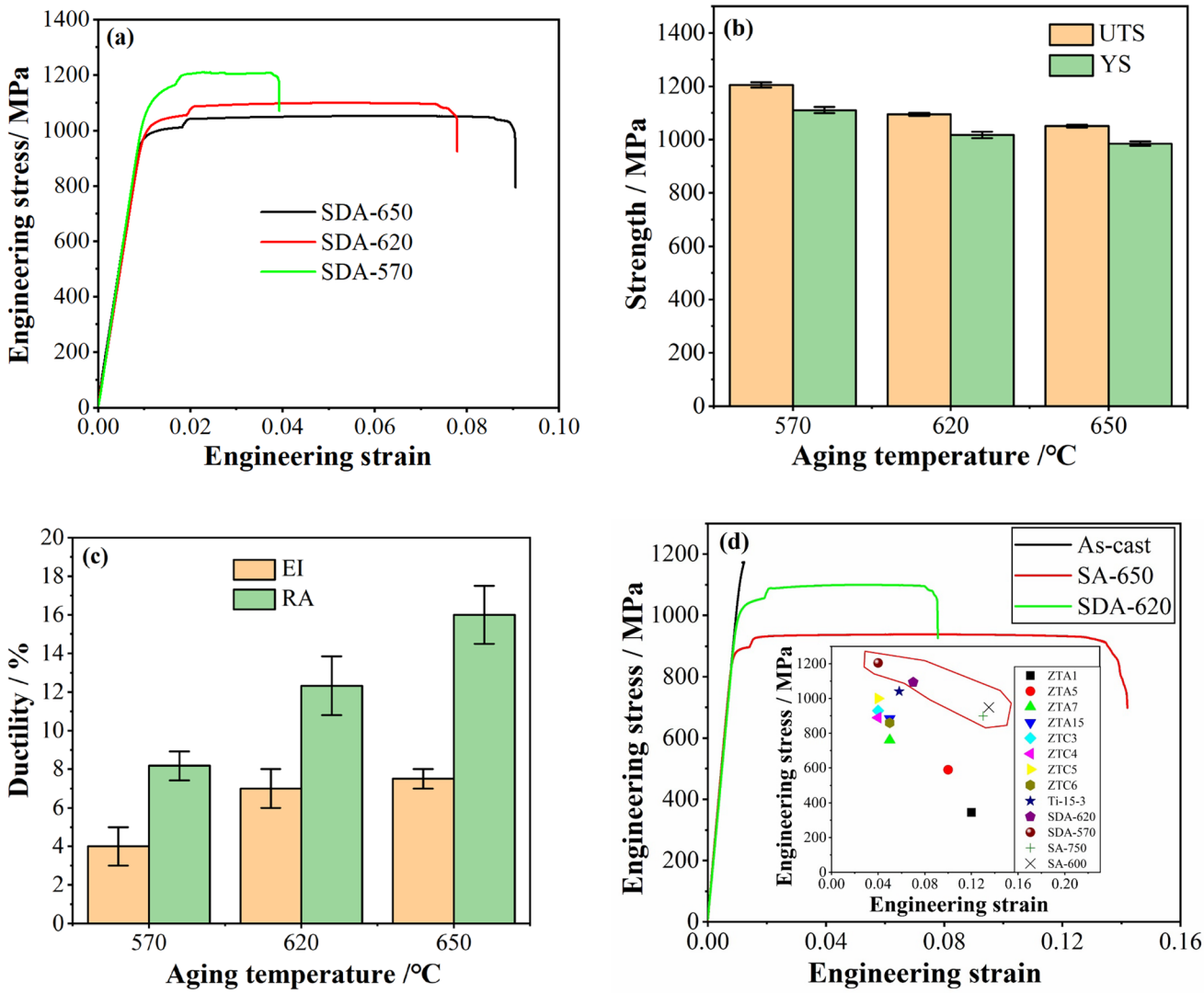

Fig. 7—Tensile properties of the Ti-1300 alloy at different secondary aging temperatures. (*a*) Stress–strain curves. (*b*) Ultimate tensile strength (UTS) and yield strength (YS). (*c*) Elongation (EI) and reduction area (RA). (*d*) Stress–strain curves of as-cast, SA-650 and SDA-620, and inserted picture in (d) shows engineering stress *vs* engineering strain of this work in comparison with typical cast titanium alloy.

influence of morphology and lamellar width of the α_S phase on mechanical properties, and the detailed post heat-treatment process parameters for samples SDA-650, SDA-620, and SDA-570 are shown in Figure 1(b). Figure 6 shows the SEM images of the investment casting Ti-1300 alloy after applying the SDA post heat-treatment. Figures 6(a) through (c) shows that the microstructures after SDA post heat-treatment are composed of the α_P phase and β_R matrix. As shown in Figure 3, the α_P phase is precipitated during the first aging at 750 °C and the morphology and volume fraction of the α_P phase is unchanged. This means that secondary aging will not affect the morphology or volume fraction of the α_P phase. To analyze the effect of the α_S phase on the properties, a high magnification SEM was used, and the results are shown in Figures 6(e), (f). A high density of the acicular α_S phases is precipitated in β_R matrix by the secondary aging treatment. The widths of the acicular α_S phases decrease with decreasing secondary aging temperature. The widths of the acicular α_S phases under these three-post heat-treatment processes corresponded to approximately 0.2, 0.13, and 0.06 μm. The nucleation and growth of the acicular α_S phase have a competitive relationship. Generally, a high aging temperature can provide a high nucleation activation energy. This means that SDA-650 sample has the maximum nucleation activation energy, which can effectively hinder the growth of the acicular α_S phase. In addition, some α_S phases are spheroidized when the secondary aging temperature is increased to 650 °C. By contrast, a high secondary aging temperature is beneficial for obtaining α_S phases with small aspect ratios.

Figure 7 shows variation in the tensile properties of the investment casting Ti-1300 alloy after SDA post heat-treatment. The UTS and YS increase with decreasing secondary aging temperatures; however, the EI and RA decrease with decreasing secondary aging temperatures. Deng *et al.*[31] report, the soft coarse α_P phase mainly provides ductility in the bimodal structural

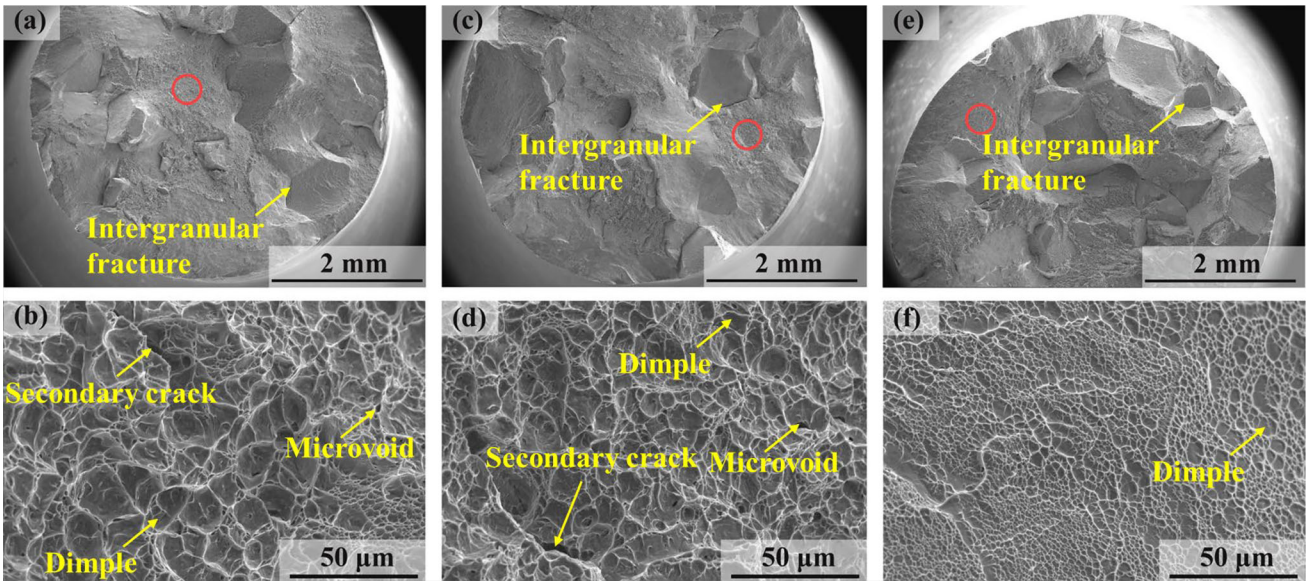

Fig. 8—Fracture morphologies of investment casting Ti-1300 alloy after SDA post heat-treatment. (*a*) and (*b*) SDA-650, (*c*) and (*d*) SDA-620, and (*e*) and (*f*) SA-570.

sample, while the fine α_S phase determine its strength. Ding *et al.*[19] think that high aging temperature can promote the growth of α_s phase in β_R matrix and the decrease in the α/β interface area in the alloy, which result in the weakening of the second phase strengthening effect. Wu *et al.*[31] believe that α/β interfaces can hinder dislocation slip between these two phases. As shown in Figure 6, we can find that as the aging temperature increases, the α_S phase volume fraction and α/β interface area decrease. Therefore, we can think that the increase of UTS and YS with decreasing secondary aging temperatures can be ascribed to the weakening of interface strengthening effect. Although high volume of α/β interfaces can enhance the interface strengthening effect, it will significantly hinder dislocation slip between these two phases and further act as stress concentrators. Additionally, thin α plates decrease the size of the plastic deformation zone of a crack tip. Therefore, The EI and RA show a decreasing trend as the aging temperature decreased. The inserted picture in Figure 7(d) shows engineering stress *vs* engineering strain of this work in comparison with typical cast titanium alloy. The investment casting Ti-1300 alloy after SA and SDA process post-treatment shows a high strength–plasticity matching relationship compared with the typical cast titanium alloy, and overcoming the strength–plastic trade-off.

To further investigate the influence of the SDA post heat-treatment on fraction behavior, the tensile fracture morphologies of these samples were investigated, as shown in Figure 8. The macroscopic morphologies of the fracture surfaces in the samples are composed of rough regions with some flat regions, marked with yellow arrows in Figures 8(a), (c), and (e). This indicates that the fracture mechanism of the investment casting Ti-1300 alloy after SDA post heat-treatment is a mixed mode of transgranular and intergranular fracturing.[31] The volume fraction of the flat regions, however, increases with decreasing secondary aging temperature, indicating that the main fracture mechanism changes from transgranular fracture to intergranular fracture. For further analysis, the rough regions in Figures 8(a), (c), and (e) (marked with red circles) were analyzed, as shown in Figures 8(b), (d), and (f), respectively. SDA-650 and SDA-620 exhibit fractured features, including dimples, microvoids, and secondary cracks; however, only dimples are observed in SDA-570. The size and depth of the dimples become smaller and shallower with decreasing secondary aging temperature. Therefore, the EI and RA of the investment casting Ti-1300 alloy decrease with decreasing secondary aging temperature. By contrast, the widths of the α_S phases decrease with decreasing secondary aging temperature, which results in an easy concentration of stress at the tip of the acicular α_S phase. After heat treatment by the SDA-620 process, the UTS, YS, EI, and RA of the investment casting Ti-1300 alloy were 1094 MPa, 1017 MPa, 7.0, and 12 pct, respectively.

IV. CONCLUSIONS

In this work, the influence of post heat-treatment methods and process parameters on the morphology and volume fraction of the α_P and α_s phases and the corresponding mechanical properties in the near-β titanium alloy Ti-1300 alloy fabricated by investment casting were studied systematically. The main conclusions are drawn as:

(1) The microstructure of as-cast Ti-1300 alloy prepared by investment casting is a typical coarse Widmanstätten structure, exhibiting high strength of 1143.0 MPa but almost zero elongation.
(2) After SA post heat-treatment, the EI and RA of investment casting Ti-1300 alloy was effectively

improved. The EI increased from 1.2 pct in the as-cast sample to 13.5 pct in the SA-600 post heat-treated sample, while also achieving a UTS of 949 MPa. These superior properties stem from the combined effects of microstructures, including grain boundary α phase, primary α phase, and α colonies.

(3) After SDA post heat-treatment of the SA-750 sample, the UTS and YS were increased further and the EI and RA decreased with decreasing secondary aging temperatures. The UTS increased from 889 MPa in SA-750 sample to 1205 MPa in the SDA-570 sample, while also achieving an EI of 4 pct.

The increase of UTS and YS with decreasing secondary aging temperatures can be ascribed to the weakening of interface strengthening effect. The EI and RA decrease with decrease of aging temperature can be ascribed to high volume of α/β interfaces can significantly hinder dislocation slip between these two phases and further act as stress concentrators. Additionally, thin α plates decrease the size of the plastic deformation zone of a crack tip.

ACKNOWLEDGMENTS

This work was supported by the Qin Chuangyuan cited the high-level innovation and entrepreneurship talent project of Shaanxi Province (QCYRCXM-2022–55).

CONFLICT OF INTEREST

The authors declare that they have no known competing financial interests or personal relationships that could have appeared to influence the work reported in this paper.

REFERENCES

1. N. Ramachandiran, H. Asgari, F. Dibia, R. Eybel, W. Muhammad, A. Gerlich, and E. Toyserkani: *J. Alloy Compd.*, 2023, vol. 938, p. 168616.
2. R.R. Boyer and R.D. Briggs: *J. Mater. Eng. Perform.*, 2005, vol. 14, pp. 680–84.
3. Y. Cui, L. Wang, and L. Zhang: *Prog. Mater. Sci.*, 2024, vol. 144, p. 101277.
4. Y. Zhang, D. Wei, Y. Chen, L. Xie, L. Wang, L.C. Zhang, W. Lu, and G. Chen: *J. Mater. Sci. Technol.*, 2024, vol. 1(186), pp. 48–63.
5. S.K. Kar, A. Ghosh, N. Fulzele, and A. Bhattacharjee: *Mater. Charact.*, 2013, vol. 81, pp. 37–48.
6. J.C. Sabol, T. Pasang, W.Z. Misiolek, and J.C. Williams: *J. Mater. Process. Technol.*, 2012, vol. 212, pp. 2380–85.
7. H. Matsumoto, M. Kitamura, Y. Li, Y. Koizumi, and A. Chiba: *Mater. Sci. Eng. A*, 2014, vol. 611, pp. 337–44.
8. B. Vrancken, L. Thijs, J.P. Kruth, and J. Van Humbeeck: *Acta Mater.*, 2014, vol. 68, pp. 150–58.
9. O.M. Ivasishin, P.E. Markovsky, Yu.V. Matviychuk, S.L. Semiatin, C.H. Ward, and S. Fox: *J. Alloy Compd.*, 2008, vol. 457, pp. 296–309.
10. O.M. Ivasishin, P.E. Markovsky, S.L. Semiatin, and C.H. Ward: *Mater. Sci. Eng. A*, 2005, vol. 405, pp. 296–305.
11. Z.S. Zhu: *J. Aeronaut. Mater.*, 2014, vol. 34, pp. 44–50.
12. C. Liu, Y. Wang, Y. Zhang, L.-C. Zhang, and L. Wang: *Int. J. Plast.*, 2024, vol. 173, p. 103884.
13. C. Liu, L. Xie, L. Zhang, and L. Wang: *Mater. Res. Lett.*, 2024, vol. 12, pp. 425–32.
14. R. Sharon Uwanyuze, J.E. Kanyo, S.F. Myrick, and S. Schafföner: *J. Alloy Compd.*, 2021, vol. 865, p. 158558.
15. Z. Er-tuan, K. Fan-tao, C. Yu-yong, and Li. Bao-hui: *Trans. Nonforrous Met. Soc. China*, 2011, vol. 21, pp. s348-352.
16. H. Clemens and S. Mayer: *Mater. High Temp.*, 2016, vol. 33, pp. 560–70.
17. Z. Liu, Z. Du, H. Jiang, X. Zhao, T. Gong, X. Cui, J. Cheng, F. Liu, and W. Chen: *J. Mater. Res. Technol.*, 2022, vol. 17, pp. 2528–39.
18. R. Wang: *Metals-Basel*, 2021, vol. 11, p. 1397.
19. H. Ding, L. Wang, X. Lin, A. Xue, L. Yuan, M. Dang, and W. Huang: *Mater. Sci. Eng. A*, 2022, vol. 855, p. 143907.
20. J.W. Lu, Y.Q. Zhao, P. Ge, H.Z. Niu, Y.S. Zhang, W. Zhang, and P.X. Zhang: *Mater. Sci. Eng. A*, 2015, vol. 621, pp. 182–89.
21. Lu. Jinwen, Y. Zhao, P. Ge, Y. Zhang, H. Niu, W. Zhang, and P. Zhang: *J. Alloy Compd.*, 2015, vol. 637, pp. 1–4.
22. H.Z. Zhao, L. Xiao, P. Ge, J. Sun, and Z.P. Xi: *Mater. Sci. Eng. A*, 2014, vol. 604, pp. 111–16.
23. X. Wen, M.P. Wan, C.W. Huang, and M. Lei: *Mater. Sci. Eng.*, 2019, vol. 740(7), pp. 121–29.
24. A. Bhattacharjee, V.K. Varma, and S.V. Kamat: *Metall. Mater. Trans. A*, 2006, vol. 37A(5), pp. 1423–33.
25. X.W. Ye, M.P. Wan, C.W. Huang, M. Lei, S.C. Jian, Y. Zhang, D. Xu, and F. Huang: *Mater. Sci. Eng. A*, 2022, vol. 840, p. 142825.
26. G.T. Terlinde, T.W. Duerig, and J.C. Williams: *Metall. Mater. Trans. A*, 1983, vol. 14A, pp. 2101–15.
27. J. Wang, X. Ye, Y. Li, M. Wan, C. Huang, F. Huang, M. Lei, D. Liu, R. Ma, and X. Ren: *Mater. Sci. Eng. A*, 2023, vol. 869, p. 144788.
28. H. Schwab, F. Palm, U. Kühn, and J. Eckert: *Mater. Des.*, 2016, vol. 105, pp. 75–80.
29. L.X. Li, Y. Lou, L.B. Yang, D.S. Peng, and K.P. Rao: *Mater. Des.*, 2002, vol. 23, pp. 451–57.
30. I. Philippart and H.J. Rack: *Mater. Sci. Eng. A*, 1998, vol. 243, pp. 196–200.
31. H. Deng, W. Qiu, S. Cao, L. Chen, Hu. Zhendong, Y. Wei, Z. Xia, L. Zhou, X. Cui, and J. Tang: *J. Alloy Compd.*, 2021, vol. 858, p. 158351.
32. G.Q. Wu, C.L. Shi, W. Sha, A.X. Sha, and H.R. Jiang: *Mater. Sci. Eng. A*, 2013, vol. 575, pp. 111–18.